

# ViCE: Improving Visual Concept Embedding Discovery in Unsupervised Semantic Segmentation by Superpixelization

Robin Karlsson<sup>1</sup>, Tomoki Hayashi<sup>1</sup>, Keisuke Fujii<sup>1</sup>, Alexander Carballo<sup>1</sup>,  
Kento Ohtani<sup>1</sup>, Kazuya Takeda<sup>1,2</sup>

<sup>1</sup>Nagoya University, <sup>2</sup>Tier IV

**Abstract.** Recent self-supervised computer vision methods have demonstrated equal or better performance to supervised methods, opening for AI systems to learn visual representations from practically unlimited data. However, these methods are classification-based and thus ineffective for learning dense feature maps required for unsupervised semantic segmentation. This work presents a method to effectively learn dense semantically rich visual concept embeddings applicable to high-resolution images. We introduce superpixelization as a means to decompose images into a small set of visually coherent regions, allowing efficient learning of dense semantics by swapped prediction. The expressiveness of our dense embeddings is demonstrated by significantly improving the SOTA representation quality benchmarks on COCO (+16.27 mIoU) and Cityscapes (+19.24 mIoU) for both low- and high-resolution images. *Code made available upon publication.*

**Keywords:** Self-supervised learning, unsupervised semantic segmentation, object discovery, superpixels, image decomposition, visual concepts



**Fig. 1.** ViCE learns dense semantic embeddings from raw image data. Here we visualize the output of a linear model interpreting the embeddings. The left and center images display output for low- and high-resolution images. The right image shows output from our comparative SOTA baseline PiCIE [19].

## 1 Introduction

Deep learning is recognized as the most potent modelling tool available for representation learning on unstructured data [4]. The universal approximation theorem theoretically proves that deep neural networks (DNN) unbounded in either depth [61] or width [46] can approximate any function arbitrarily well.

Progress in general computer vision tasks in the past decade has been based on supervised learning with large datasets annotated by human labelers [51]. Arguments are made that generalizable and robust computer vision models has not yet been achieved, and further increasing the amount of labeled data is unsustainable [22,63]. One hypothesis is that learning from top-down categorization (“what it *is*”) from semantically vague and inconsistent human annotation could be limiting our pursuit of robust computer vision [31]. Instead, cognitive science tells us that learning through bottom-up association (“what it is *like*”) may be more similar to how visual concepts emerge for humans [80,64,69,70]. The success of bottom-up learning for word embeddings in natural language processing (NLP) [43,65,66] further strengthens the hypothesis.

Recent self-supervised computer vision methods show promise in this direction, as results are gradually approaching or even surpassing the performance of supervised methods [37]. However, these methods are classification-based and thus ineffective for learning dense feature maps required for unsupervised semantic segmentation.

In this paper we explain how to train a model to represent images as a semantically rich feature map of latent **visual concept embeddings** (ViCE). Our working hypothesis is that there exists a strong analogy between how image context defines the meaning of pixel regions, and how sentence context defines the meaning of categorical word tokens [43]. We view the generation of natural images as a stochastic process. Supposing a set of latent visual concepts give rise to observable pixel appearances, we formulate our method to learn the inverse mapping from observed pixels to latent visual concepts through self-supervised learning. The learning signal originates from the inherent contextual and appearance invariances, and geometric equivariance, of entities with permanence the observable world.

A core component of our method is to decompose images into a small set of visually coherent regions using superpixelization. Our experiments show how the resulting complexity reduction improves the effectiveness and efficiency of classification-based self-supervised vision methods for the dense semantic segmentation task.

Our motivation for advancing unsupervised semantic segmentation its relevance to the problem of probabilistic computer vision. By partitioning images into a small set of semantic visual concept embeddings, theoretically it is possible to realize tractable probabilistic enumeration of possible configuration spaces for images. We also see our work as a contribution towards a practical solution to the symbolic grounding problem [42] in vision.

The contributions of our paper are as follows:

- A new conceptual approach to represent high-resolution images as semantically rich embedding maps partitioned into distinct, coherent regions, represented by a latent **visual concept embedding** (ViCE), analogous to word embeddings in NLP.
- The first work to introduce superpixelization for self-supervised computer vision, as a simple yet effective natural hierarchical decomposition from pixels to a small set of visually coherent regions.
- Experimentally demonstrate that superpixelization improves both results and reduce computational time for learning embedding maps, and that superpixels are more effective than conventional grids. We also introduce the benefit of masking for unsupervised semantic segmentation.
- We implement a densification of the self-supervised swapped prediction method [12], and experimentally verify the algorithms effectiveness for learning dense embedding maps.
- Present extensive experiments and SOTA results for unsupervised semantic segmentation benchmarks on COCO (+16.27 mIoU) and Cityscapes (+19.24 mIoU). Our method is able to learn better or equally well from high-resolution images, in contrast to prior methods.

## 2 Related work

**Self-supervised representation learning** Many early works in applying self-supervised methods for computer vision focus on learning to solve pretext tasks as a substitute for human annotations [29,74,68,7,34,100]. However, recent work [17,44] demonstrates that image-level embedding classification with cross-entropy minimization on large datasets [26,57] is a more effective approach capable of surpassing supervised pretraining [37,13]. Contrastive methods [17,71,44] learn discriminative latent embedding vectors for images by “pulling together” views of the same image, and “pushing away” embeddings of different images. Recent non-contrastive methods [98,40,13] demonstrate approaches to avoid negative sampling to improve computational efficiency. Clustering methods [10,2,12,11,99,95] simultaneously discovers a set of clusters or prototypes, and learns discriminative image embeddings suitable for clustering. Contrary to contrastive methods, the objective does not have to be approximated as optimizing over the relatively small set of negative representative clusters is tractable. DeepCluster [10] iteratively performs K-means clustering over the entire dataset and learns an embedding model and classification head to predict the K-means cluster assignment. SeLA [2] presents a principled formulation for clustering and representation learning as a single optimization objective, by casting cluster assignment as an optimal transport problem [54,23]. SwAV [12] and ODC [99] demonstrate that clustering can be done online per batch to increase learning efficiency. Our method increases the effectiveness of dense representation learning for images by introducing superpixelization as a simple yet efficient image decomposition technique. We obtain better results on low-resolution images, and also achieve comparable results for high-resolution images, unlike prior methods.

**Self-supervised computer vision** Recently self-supervised representation learning is being applied beyond classification to vision tasks involving explicit representation of spatial information. In object detection [3,89,94,24,88,92] self-supervision is generally used to learn expressive embeddings for plausible object proposal regions sampled randomly or heuristically [85]. Comparatively few works exist for semantic segmentation, as naively applying classification-based self-supervised methods to learn dense pixel-level embedding maps with millions of vectors is challenging. Existing works leverage self-supervised clustering approaches to learn coherent semantic groupings from pixels [19,48,72], autoregressive modeling [72], and GAN-based approaches [16,5]. Other works [47,87] leverages self-supervised depth map estimation [35,62] for enhancing semantic segmentation performance. Recently, DINO [13] demonstrated that attention maps for “things” naturally emerge for self-supervised Vision Transformer (ViT) models [30,86]. Our work improves the efficiency of self-supervised methods for dense pixel-level representation learning, as well as extending capability to high-resolution images. Unlike attention maps, our model partitions the entire image into embeddings for both “things” and “stuff”.

**Word embeddings and visual tokens** In natural language processing (NLP), the basic representation of words are categorical tokens or one-hot vectors. Learning semantic embeddings for words using unsupervised methods as a pre-training task [65,66,76] offers significant improvements for downstream tasks compared with learning word embeddings as part of the task [84]. Word embeddings is the de facto elementary representation used by all recent language models [27,52,96,58]. The metric of semantic similarity between words is co-occurrence in sentences [43]. Embedding models are optimized so that the embeddings for two words that often co-occur is close in vector space. A separate set of sampled word embeddings assumed to be unrelated are pushed away similarly to noise contrastive estimation [41,71] to avoid degenerate solutions [36]. Our work is inspired by the idea of word co-occurrence. Our method is based on discovering co-occurring abstract pixel patterns within a common image subregion of augmented views with different context and pixel appearance.

In computer vision, the bag of visual words model [83,32,82] decompose images into discriminative local image features typically extracted at keypoint locations by a SIFT detector [60]. Later works propose to discover mid-level visual elements or words with richer visual semantics in the form of discriminative patches [81] and mode seeking [28] based on learning through iterative clustering and classification similar to recent self-supervised clustering methods [10] but for representative HOG features [25] in pixel space. More recently, extraction of latent embeddings or tokens for image patches is demonstrated by prior GNN methods [18,101,55]. The Visual Transformer (VT) [91] adds recurrence to generate visual tokens from current and previous spatial attention maps. However, these methods require a separate transformation matrix to be learned through dense supervised learning task. Unlike VT, our method learns to generate se-

mentally rich visual embedding maps without requiring a secondary supervised task.

### 3 ViCE: Visual Concept Embeddings

The concept of “the thing in itself” in Kantian philosophy, or noumena in general, denotes the existence of objects as they are independent of observation. Similarly, one can view the generation of natural images perceived by a photometric sensor to be generated from a set of latent semantic visual concepts by a generative process. We model this process by a generative model  $f$  with two conditional variables. First, a set of latent visual concepts  $C = (c^{(1)}, \dots, c^{(K)})$ , encoded into a dense embedding map  $Z$ , to represent entities beyond particular pixel appearances. Secondly, a set of latent sensing parameters  $S$ , representing the sensing environment and intrinsic parameters of a sensor. The model  $f$  generates the observable pixel appearance  $X$  of entities. As the exact sensing parameters are not inferrable, the generative model  $f$  becomes a stochastic model  $P$ .

$$f(X|Z, S) \approx P(X|Z) \quad (1)$$

This work presents a self-supervised method named ViCE, for learning dense and semantically rich **visual concept embeddings** for images. The method is based on learning an approximate function  $f_\theta$  for the inverse mapping  $P^{-1}(Z|X)$  from observed pixels  $X$  to the latent visual embedding map  $Z$ , while simultaneously discovering a set of latent visual concept  $C$ .

Discovery of latent visual concepts is made possible by identifying a set of co-occurring high-level abstract pixel patterns, generated from images with different visual context. We relate our approach to discover the semantic meaning for pixels, to the discovery of semantic meaning for words in NLP. Methods to learn semantically rich word embeddings [65,66,76] are based on co-occurrence [43] and context [27,77] of individually meaningless tokens, akin to our approach.

We propose to learn a mapping  $f_\theta$  that predicts the same visual concept embedding map  $Z$  for the same mutually co-occurring abstract pixel patterns generated from augmented views  $\tilde{X}^{(m)}$ . All views contains one subregion representing the same content, but with different pixel appearance and surrounding context.

$$f_\theta(\tilde{X}^{(m)}) \simeq Z \quad \forall m \in (1, \dots, M) \quad (2)$$

The visual concept vectors  $c \in \mathbb{R}^D$  are constrained to lie on the surface of a  $D$  dimensional unit hypersphere. Each dimension presumably corresponds to a distinct visual concept primitive or basis vector, and visual concepts are linear combinations of these primitives. The set of concepts  $C$  are known and finite, theoretically allowing tractable probabilistic enumeration over possible configuration akin to successful probabilistic language modelling approaches in NLP [27,78].

We apply the successful self-supervised learning method SwAV [12] to learn both the mapping function  $f_\theta$  and the set of concepts  $C$ , though in principle any

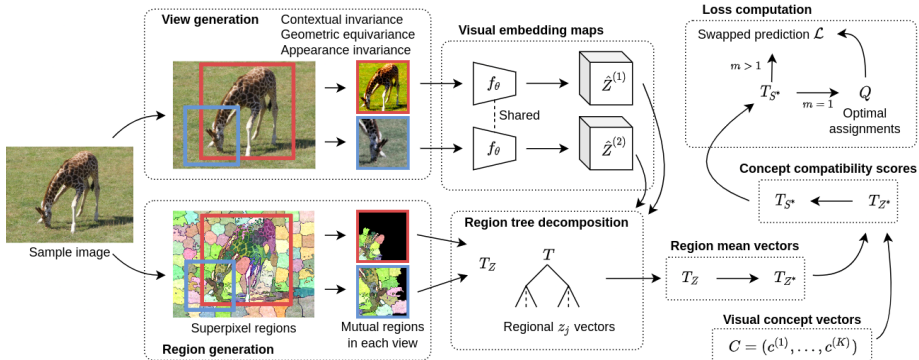


**Fig. 2.** Overview of ViCE. A training iteration starts by generating  $M$  augmented views. First, we partition the image into  $I$  mutually common superpixel regions. The model  $f_\theta$  transforms view images into visual concept embedding maps  $\hat{Z}^{(m)}$ . All vectors  $z_j$  for each element  $j$  of region  $i$  in view  $m$  of image  $n$  are gathered in the tree structure  $T_Z$ . A mean vector  $z_i^*$  is computed from all vectors  $v_j$  for each region  $i$ . Next, we score each  $z_i^*$  in terms of closeness to each concept vector  $c^{(k)}$ , resulting in region-specific score vectors  $s_i^*$ . The swapped prediction objective  $\mathcal{L}$  generates learning gradients.

cluster-based self-supervised method [10,2,11,99] can be used. Fig. 2 shows an overview of our method.

### 3.1 Decomposing images into coherent regions

A high-resolution image contains millions of individually meaningless and mostly redundant pixels. However, it is known that training on high-resolution images is beneficial for learning to segment small objects such as poles and pedestrians [14]. Nevertheless, naively applying vector comparison based self-supervised representation learning methods on high-resolution embedding maps is inefficient as well as ineffective. To solve this problem, we propose to decompose the image into a small set of visually coherent regions using superpixelization [79].

Superpixel methods like Simple Linear Iterative Clustering (SLIC) [1] are adept at  $\mathcal{O}(1000)$  complexity reductions, transforming an image from millions of pixels into less than a thousand regions. In contrast to image decomposition by a grid, as done in recent works based on Vision Transformer (ViT) models [30,13], superpixels are capable of preserving detail by representing thin and small pixel patches like poles as distinct regions.

### 3.2 View generation

The following sections explain central aspects of how we generate augmented views for discerning the latent semantic visual concepts through pixel appearance invariance [17], geometric equivariance [19], and contextual invariance. Two augmented views are shown in Fig. 3.



**Fig. 3.** Examples of two generated view pairs. The first image displays the actual view feed to the model. The second image illustrates the mutual image region. The third image shows mutual superpixel regions colored by region index.

To generate views with different context, we first sample a center point  $(x, y)^*$  in the image. Sampling is done in content-rich regions to better satisfy the equipartitioning of concepts assumption [2,12] for each training batch. We found that probabilistic sampling from a Gaussian filtered Canny edge detection map[9] is a useful measure of image content. Views  $\tilde{X}^{(m)}$  are generated by sampling  $M$  view centers  $(x, y)^{(m)}$  around  $(x, y)^*$  while ensuring a mutual image subregion exists.

We generate geometrically equivariant views by first sampling a resize coefficient  $\beta^{(m)}$  for each view  $m$ .  $\beta$  determines the size of the cropped out view region as exemplified by the red and blue crop regions in Fig. 2. All view crops are resized to the common view size, thus enforcing the model to learn resolution invariant representations. All views are randomly flipped horizontally.

All views are augmented by random color distortion and Gaussian blurring before normalization to learn appearance invariant visual concepts [17,93,90]. A ratio of superpixel regions are masked with noise as a means to learn robust features and alleviate the shortcut learning problem [33].

### 3.3 Learning algorithm

The swapped prediction learning objective [12]  $\mathcal{L}$  is designed to simultaneously learn the mapping function  $f_\theta$  in Eq. 2, and optimize the distribution of latent visual concepts  $C$ . The algorithm can be viewed as an extension of SwAV [12] to the problem of learning dense embedding maps. We refer to prior work for an explanation of SwAV itself [12,2,23,50]. The rest of this section explains the flow of a training iteration as visualized in Fig. 2. We provide pseudocodes in the supplementary material.

A training iteration starts by randomly sampling  $N$  images  $X^{(n)} \in \mathbb{R}^{3 \times H \times W}$  with height  $H$  and width  $W$ . Each image is partitioned into superpixel regions represented as matrices  $A^{(n)} \in \mathbb{R}^{H \times W}$ , with values specifying the pixel’s region index. Next, a set of  $M$  augmented views  $\tilde{X}^{(n)} = \{\tilde{X}^{(1,n)}, \dots, \tilde{X}^{(M,n)}\}$  are generated for each image  $X^{(n)}$  as explained in Sec. 3.2. Here  $h$  and  $w$  denotes the common view size. The superpixel matrices  $A^{(n)}$  are transformed identically to the corresponding views. The resulting set of superpixel view crops  $\tilde{A}^{(n)} = \{\tilde{A}^{(1,n)}, \dots, \tilde{A}^{(M,n)}\}$  contains only mutual regions existing in all views, as exemplified in Fig. 3. Finally the set of all views  $\tilde{X}^{(m,n)}$  are concatenated

into single tensor  $\tilde{X} \in \mathbb{R}^{B \times 3 \times h \times w}$  where  $B = NM$  denotes the total number of views.

The learned function  $f_\theta$  transforms  $\tilde{X}$  into a normalized visual embedding tensor  $\hat{Z} \in \mathbb{R}^{B \times D \times h \times w}$ . Next  $\hat{Z}^{(b)}$  is decomposed region-wise into row vectors  $\hat{z}_j \in \mathbb{R}^D$  and stored in a tree structures  $T_Z$  index by region  $i$  in view  $m$  of image  $n$ . Vectors of non-mutual regions are discarded. A single mean vector  $z^{(i,m,n)*}$  is computed to represent each region  $i$  and stored in tree  $T_{Z^*}$ . Finally each vector  $z^{(i,m,n)*}$  is scored in terms of compatibility or closeness to each visual concept vector  $C = (c^{(1)}, \dots, c^{(K)})$  by computing the following matrix product

$$s^* = (z^*)^T C \quad (3)$$

with  $C \in \mathbb{R}^{D \times K}$  represented as a matrix. Note that the cosine distance between vectors  $z$  and  $c$  equals the dot product  $z \cdot c$  as both vectors are normalized.

The learning objective  $\mathcal{L}_{cl}$  is formulated as a swapped prediction problem [12]. The score vectors  $s^{(i,m)*}$  for each region  $i$  in all secondary views  $m > 1$  are used to predict the optimal assignment of concepts  $q^{(i)}$  [12] in the primary view  $m = 1$

$$\mathcal{L}_{cl} = -\frac{1}{NM} \sum_{n=1}^N \sum_{m=2}^M \frac{1}{I} \sum_{i=1}^I q^{(i)} \log \sigma \left( \frac{1}{\tau} s^{(i,m)*} \right) \quad (4)$$

where  $\sigma()$  is the softmax function. We compute  $q^{(i)}$  efficiently by the Sinkhorn-Knopp algorithm [2,23]. A FIFO queue of accumulated  $s^{(i,1)*}$  vectors is used to improve the empirical approximation of a uniform distribution of concepts [2,12].

## 4 Experiments

We implement ViCE in the self-supervised learning framework VISSL [39] based on PyTorch [73]. The quality of learned embeddings are evaluated on the standard COCO-Stuff164k [57,8] and Cityscapes [21] benchmark datasets. The task is semantic segmentation using a linear classification model, or a clustering-based model, implemented in the framework MMSegmentation [20]. In the case of COCO, evaluation is performed on a reduced set of 27 classes obtained by merging the original 172 semantic classes following [48]. We use the conventional 27 classes for Cityscapes. Our comparative baseline for dense representation learning is the recent SOTA unsupervised semantic segmentation model PiCIE [19] based on DeepCluster [10]. Further evaluations on other downstream tasks are provided in the Supplementary.

### 4.1 Implementation details

We evaluate our method on different ResNet backbones [45] with two different decoder architectures; the SOTA semantic segmentation model DeepLabV3+ [15], and the Feature Pyramid Network (FPN) [56]. The later decoder is also used in the comparative baseline. Our model generates visual embeddings maps  $Z \in$



$\mathbb{R}^{D \times H \times W}$  with the same spatial resolution as the input image. Two embeddings  $z^{(a)}$  and  $z^{(b)}$  are compared for semantic similarity using the dot product  $\hat{z}^{(a)} \cdot \hat{z}^{(b)}$  on normalized vectors. This operation is equivalent to comparing two word embeddings by cosine distance [66,65].

## 4.2 Training Details

We conduct experiments on 32 V100 32 GB GPUs distributed over eight nodes. Each GPU loads four images, and generates five augmented views. High- and low-resolution views correspond to  $400 \times 400$  pixels and  $256 \times 256$  pixels, respectively. The resulting total batch size is 128 images with 640 views. To generating superpixels, we use SLIC [1] implemented in OpenCV [6] with average region size 20 px, smoothness factor (i.e. ruler) 10, and optimize for 5 iterations. Maximal mask coverage is 25 % with a minimum common superpixel region preservation ratio of 25 %. The view resize coefficients  $\beta$  are sampled between 0.5 to 2. The embedding dimension  $D$  and number of visual concepts  $C$  are 128 unless stated otherwise. We use the same set of hyperparameters in all benchmarking experiments. An additional hyperparameter study is given in the supplementary material.

Parameters for the clustering objective  $\mathcal{L}_{co}$  are the same as SwAV [12]. We set temperature  $\tau$  to 0.1, the regularization parameter  $\epsilon$  to 0.05, and do 3 iterations for the Sinkhorn-Knopp optimization algorithm [23]. The FIFO queue consists of 5K score vectors  $s^*$  per GPU. The model is optimized using the LARS optimizer [97] with weight decay  $10^{-6}$ . The learning rate (LR) schedule consists of a linear warmup phase followed by cosine decay [59,67]. We set the peak LR using the linear LR scaling rule [38] with a base LR 0.04 for a single node.

Most experiments use models initialized with the default ImageNet-pretrained weights to conserve computational resources. However, in Table 1 we demonstrate that ViCE can be trained from scratch and achieve better results than prior SOTA models initialized with pretrained weights.

## 4.3 Representation quality experiments

All experiments are conducted in the following manner. First, a ViCE model is trained on raw images. Next, a evaluation model is trained to map the learned ViCE model output to semantic segmentation classes. One can liken this process as learning to interpret the general visual concept embeddings in terms of a specific task. We primarily use  $1 \times 1$  convolutions without a nonlinear activation function as linear evaluations models. We also implement a cluster-based evaluation model for comparison with the baseline. First, a set of  $C$  clusters are computed based on output embeddings. Next, each cluster is assigned the label class which most frequently occupies the cluster’s pixels. All models are trained and evaluated on a separate train and validation set. See Fig. 6 for output visualizations.

We note that the two evaluation approaches have dissimilarities and similarities. The clustering approach starts out task-agnostic, as clusters are computed

**Table 1.** Representation quality experiment results on low-resolution images

Embedding extractor	mIoU	Acc.	Embedding extractor	mIoU	Acc.
<i>COCO</i>			<i>Cityscapes</i>		
IIC [48]	6.71	21.79	IIC [48]	6.35	47.88
Mod. DeepCluster [19]	9.79	32.21	Mod. DeepCluster [19]	7.06	40.67
PiCIE (C = 27) [19]	13.84	48.09	PiCIE (C = 27) [19]	12.31	65.50
PiCIE (C = 45) [19]	14.36	49.99	ViCE (C = 27)	21.48	76.45
PiCIE (L) [19]	14.77	54.75	ViCE (L = 27)	27.51	85.40
ViCE (C = 45)	12.32	52.11	<b>ViCE (L = 256)</b>	<b>31.55</b>	<b>86.33</b>
ViCE (C = 128)	19.66	59.60	ViCE (from scratch)	24.84	82.99
ViCE (L = 27)	23.63	62.07			
ViCE (L = 45)	24.09	62.26			
ViCE (L = 128)	25.08	62.96			
<b>ViCE (L = 256)</b>	<b>25.49</b>	<b>62.78</b>			

without guidance from the task, and are subsequently assigned the best-fit class by task guidance. In contrast, the linear model approach learns to directly interpret embeddings with task guidance. As both models are linear in nature, and the purpose of unsupervised semantic segmentation is ultimately to perform a task, we believe it is fair to consider the linear evaluation approach which maximizes performance. Additionally, the number of clusters and number of  $1 \times 1$  filters are analogous, as both represent linear mappings with expressivity equal to the cluster or filter count.

We also note that for evaluation, the visual concepts learned by ViCE during training are not used for evaluation, only the embeddings. It is therefore fair to compare ViCE and baseline performance as long as the number of clusters or filters are the same in both evaluation models.

**Low-resolution image experiments** Table 1 presents results for models trained and evaluated on low-resolution COCO-Stuff164k [8,57] images. ‘‘C’’ and ‘‘L’’ denotes cluster and linear model based evaluation, respectively. The number indicate number of clusters or linear filters. Both ViCE and PiCIE [19] use the same ResNet 18 backbone, FPN decoder, and  $320 \times 320$  px image downsampling procedure for fair comparison. All ViCE COCO models are trained for 4 epochs. The ViCE Cityscapes models are trained for 24 epochs. The results show that ViCE generate more representative embeddings. The results show that our embeddings are particularly suitable for linear model interpretation compared with PiCIE, for which both clustering and the linear model show comparable performance. For clustering-based evaluation, ViCE appears adept at utilizing a larger amount of clusters, while PiCIE demonstrably performs better with a few clusters. For both linear model and clustering-based evaluation performance increase with linear model size, indicating a large information content directly readable from the embeddings. We provide a visualization of a linear model and

baseline output in Fig. 1. A cluster-based evaluation example is shown in Fig. 5. Further visualizations are provided in the Supplementary.

Table 1 presents results on low-resolution Cityscapes [21] images following the same COCO-Stuff164k experiment setup. Both ViCE and PiCIE are trained with 27 clusters. ViCE is trained for 24 epochs and evaluated on the standard 27 Cityscapes classes. The results again greatly improves on the baseline.

We provide an ablation study in Table 2 to evaluate the significance of each contribution in the case of low-resolution images. The first column correspond to the baseline model using an ResNet 18 backbone with an FPN decoder [56]. The second column represent barebone ViCE implementing swapped prediction optimization [12,2]. The following two columns indicate gains from adding random masking and contextual invariance data augmentation. The fourth and fifth column shows gains from applying grid and superpixel decomposition. The final column indicates that utilizing the more complex DeepLabV3+ decoder [15] (DLV3+) is detrimental in the case of low-resolution images.

**Table 2.** Ablation study on low-resolution Cityscapes

	PiCIE	ViCE 1px	Masking	Grid 10px	Super 10px	DLV3+
mIoU	14.77	29.66	30.42	31.30	<b>31.55</b>	11.56
Time	—	34h 4min	31h 6min	5h 31min	<b>5h 31min</b>	5h 37min

**High-resolution image experiments** Table 3 showcase results obtained with ViCE on original high-resolution images. All experiments use the DeepLabV3+ decoder [15] with different backbones. The results demonstrate how ViCE achieves comparable performance on both high- and low-resolution images. By contrast, prior methods are only demonstrated to work on low-resolution images [19,48]. We also observe that ViCE is capable to scale with increased model capacity given sufficient training data, as demonstrated by the COCO results.

**Table 3.** Representation quality experiment results on high-resolution images

Backbone	Ep	mIoU	Acc.	Backbone	Ep	mIoU	Acc.
<i>COCO</i>				<i>Cityscapes</i>			
RN 50	16	29.38	67.73	RN 18	48	<b>30.40</b>	<b>87.00</b>
RN 101	12	30.66	<b>68.78</b>	RN 50	72	28.77	86.54
RN 152	12	<b>31.04</b>	68.51	RN 101	72	25.26	82.85

We provide an ablation study in Table 4 to evaluate the significance of each contribution in the case of high-resolution images. The first column is empty as learning dense embeddings over pixels in high-resolution images is intractable. The second column shows that introducing superpixelization enables learning as the number of elements is reduced by  $\mathcal{O}(1000)$ , making the problem computationally tractable. The third column demonstrates the importance of utilizing a decoder designed to segment high-resolution images such as the DeepLabV3+ decoder [15]. The final column show how using content fitting superpixels improves performance compared with an conventional structured grid with equivalent base element size.

**Table 4.** Ablation study on high-resolution Cityscapes

	FPN 1px	FPN super 20px	DLV3+ grid 20 px	DLV3+ super 20px
mIoU	—	8.98	25.53	<b>29.38</b>
Time	<i>Intractable</i>	4h 55min	10h 1min	<b>6h 16min</b>

**Superpixel vs. grid experiments** The left plot in Fig. 4 demonstrates consistent gains from using superpixels instead of grids. The right plot shows how performance converge for very small and large base element sizes. The result indicate that there exist a sweet spot for base element size in terms of effective learning in a computational time.

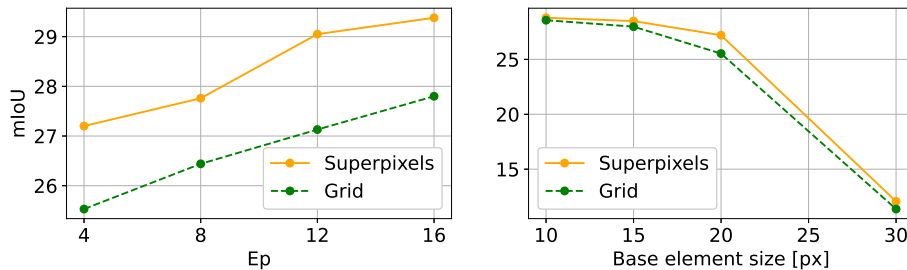


**Fig. 4.** Superpixel and grid performance compared on high-resolution COCO

**Qualitative evaluation** Fig. 5 visualizes a dense embedding maps to demonstrates how ViCE discovers distinct, consistent, and precise semantic visual entities or concepts from natural images without human supervision or heuristical

proposals [85,3]. For example, trees are represented differently from the ground, and human faces and bodies have a discernible common hue, indicating their semantic commonality. We visualize embedding maps by linearly reducing the dimensionality of each vector  $z$  using PCA [75] and rescale values to the RGB range.

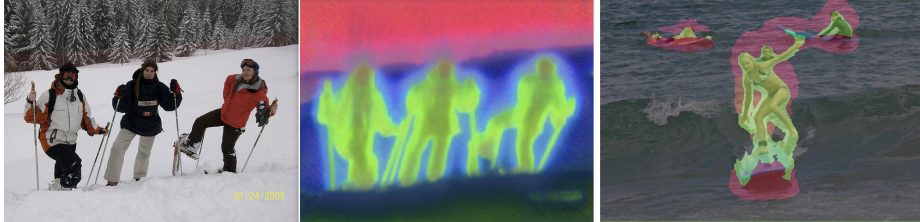


**Fig. 5.** The center figure show output embeddings visualized in RGB colors. The right figure shows output of ViCE with the clustering-based evaluation model.

## 5 Conclusion

In summary, we present a new SOTA self-supervised representation learning method ViCE for dense embedding maps. Our experiments show how decomposing images by superpixelization improves effectiveness and efficiency of classification-based self-supervised methods, in particular for high-resolution images. We also quantitatively demonstrate how superpixels achieve better performance than conventional grid decomposition. Our method exceeds the baseline performance when evaluated by both linear and cluster-based models. While the prior SOTA method [19] achieves comparable results for clustering and linear model evaluation, we find that ViCE excels in particular with linear models. As linear models allow for a task-specific interpretation of individual features, in contrast to task-agnostic clustering, we take this as further evidence for the enhanced expressiveness of our embeddings.

We hope our method will contribute towards further bridging recent success in self-supervised computer vision to the dense unsupervised semantic segmentation literature. We also believe partitioning an image into a set of visual concepts is relevant to the future advancement of probabilistic computer vision [53] and the symbolic grounding problem [42].

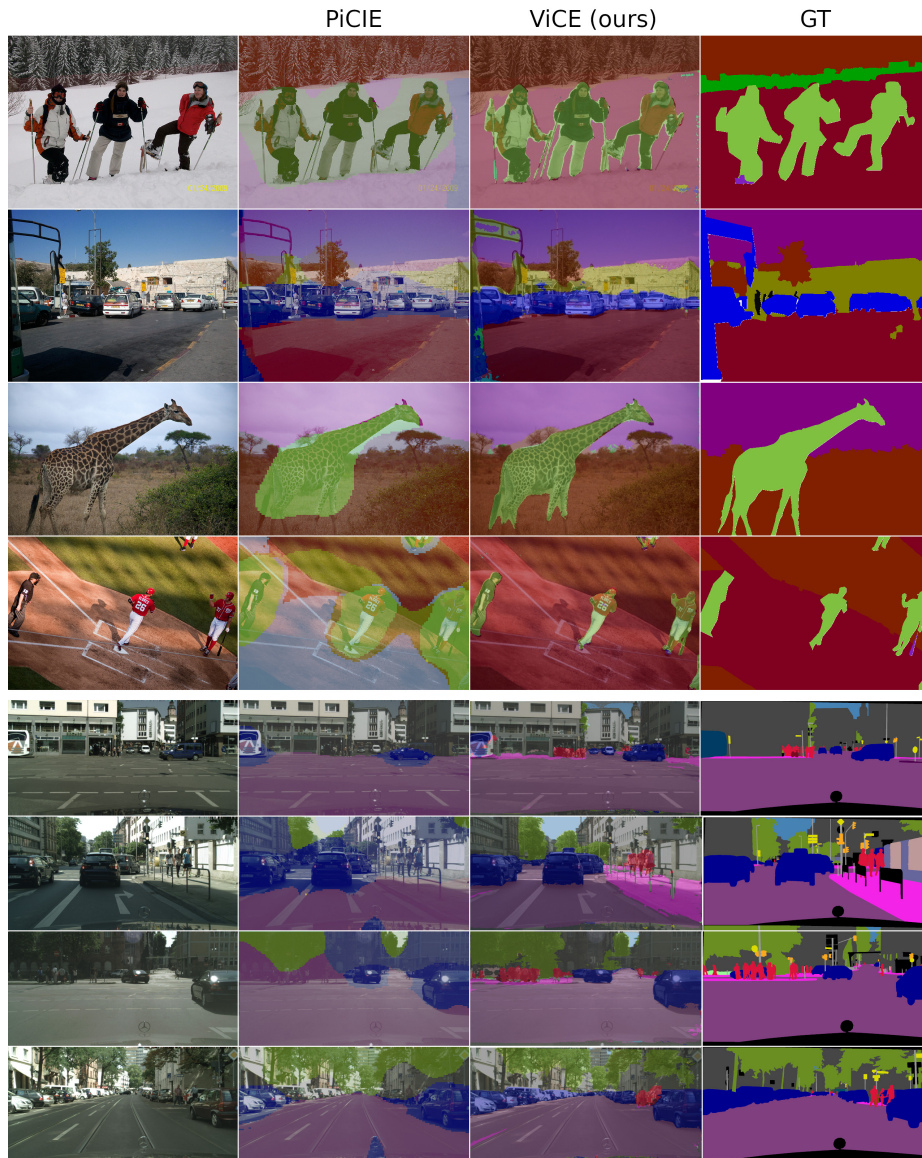


Fig. 6. Output visualizations on COCO (top) and Cityscapes (bottom)

## References

1. Achanta, R., Shaji, A., Smith, K., Lucchi, A., Fua, P., Süsstrunk, S.: SLIC superpixels. In: EPFL Technical Report. vol. 149300 (2010)
2. Asano, Y.M., Rupprecht, C., Vedaldi, A.: Self-labelling via simultaneous clustering and representation learning. In: ICLR (Apr 2020)
3. Bar, A., Wang, X., Kantorov, V., Reed, C., Herzig, R., Chechik, G., Rohrbach, A., Darrell, T., Globerson, A.: DETReg: Unsupervised pretraining with region priors for object detection. ArXiv **abs/2106.04550** (2021)
4. Bengio, Y., Courville, A., Vincent, P.: Representation learning: A review and new perspectives. *IEEE Transactions on Pattern Analysis and Machine Intelligence (TPAMI)* **35**(8), 1798–1828 (2013)
5. Bielski, A., Favaro, P.: Emergence of object segmentation in perturbed generative models. In: NeurIPS. vol. 32 (2019)
6. Bradski, G.: The OpenCV Library. *Dr. Dobb’s Journal: Software Tools for the Professional Programmer* **25**(11), 120–123 (2000)
7. Bucci, S., D’Innocente, A., Liao, Y., Carlucci, F.M., Caputo, B., Tommasi, T.: Self-supervised learning across domains. *IEEE Transactions on Pattern Analysis and Machine Intelligence (TPAMI)* (2021). <https://doi.org/10.1109/TPAMI.2021.3070791>
8. Caesar, H., Uijlings, J., Ferrari, V.: COCO-Stuff: Thing and stuff classes in context. In: CVPR. pp. 1209–1218 (2018)
9. Canny, J.F.: A computational approach to edge detection. *IEEE Transactions on Pattern Analysis and Machine Intelligence (TPAMI)* **PAMI-8**(6), 679–698 (1986)
10. Caron, M., Bojanowski, P., Joulin, A., Douze, M.: Deep clustering for unsupervised learning of visual features. In: ECCV (2018)
11. Caron, M., Bojanowski, P., Mairal, J., Joulin, A.: Unsupervised pre-training of image features on non-curated data. In: ICCV. pp. 2959–2968 (2019). <https://doi.org/10.1109/ICCV.2019.00305>
12. Caron, M., Misra, I., Mairal, J., Goyal, P., Bojanowski, P., Joulin, A.: Unsupervised learning of visual features by contrasting cluster assignments. In: NeurIPS. vol. 33 (2020)
13. Caron, M., Touvron, H., Misra, I., Jegou, H., Mairal, J., Bojanowski, P., Joulin, A.: Emerging properties in self-supervised vision transformers. In: ICCV. pp. 9650–9660 (2021)
14. Chen, L.C., Papandreou, G., Kokkinos, I., Murphy, K.P., Yuille, A.L.: DeepLab: Semantic image segmentation with deep convolutional nets, atrous convolution, and fully connected CRFs. *IEEE Transactions on Pattern Analysis and Machine Intelligence (TPAMI)* **40**, 834–848 (2018)
15. Chen, L.C., Zhu, Y., Papandreou, G., Schroff, F., Adam, H.: Encoder-decoder with atrous separable convolution for semantic image segmentation. In: ECCV. pp. 833–851 (2018)
16. Chen, M., Artières, T., Denoyer, L.: Unsupervised object segmentation by re-drawing. In: NeurIPS. vol. 32, pp. 12705–12716 (2019)
17. Chen, T., Kornblith, S., Norouzi, M., Hinton, G.E.: A simple framework for contrastive learning of visual representations. In: ICML. pp. 1597–1607 (2020)
18. Chen, Y., Rohrbach, M., Yan, Z., Yan, S., Feng, J., Kalantidis, Y.: Graph-based global reasoning networks. In: CVPR. pp. 433–442 (2019)
19. Cho, J.H., Mall, U., Bala, K., Hariharan, B.: PiCIE: Unsupervised semantic segmentation using invariance and equivariance in clustering. In: CVPR. pp. 16794–16804 (2021)

20. Contributors, M.: MMSegmentation: Openmmlab semantic segmentation toolbox and benchmark. <https://github.com/open-mmlab/msegmentation> (2020)
21. Cordts, M., Omran, M., Ramos, S., Rehfeld, T., Enzweiler, M., Benenson, R., Franke, U., Roth, S., Schiele, B.: The Cityscapes Dataset for semantic urban scene understanding. In: CVPR. pp. 3213–3223 (2016)
22. Cunn, Y.L.: Self-supervised learning (keynote talk). AAAI (2020)
23. Cuturi, M.: Sinkhorn distances: Lightspeed computation of optimal transport. In: NeurIPS. vol. 26, pp. 2292–2300 (2013)
24. Dai, Z., Cai, B., Lin, Y., Chen, J.: UP-DETR: Unsupervised pre-training for object detection with transformers. In: CVPR. pp. 1601–1610 (2021)
25. Dalal, N., Triggs, B.: Histograms of oriented gradients for human detection. CVPR **1**, 886–893 (2005)
26. Deng, J., Dong, W., Socher, R., Li, L.J., Li, K., Fei-Fei, L.: ImageNet: A large-scale hierarchical image database. In: CVPR. pp. 248–255 (2009)
27. Devlin, J., Chang, M.W., Lee, K., Toutanova, K.: BERT: Pre-training of deep bidirectional transformers for language understanding. In: NAACL. pp. 4171–4186 (2019)
28. Doersch, C., Gupta, A., Efros, A.A.: Mid-level visual element discovery as discriminative mode seeking. In: NIPS. pp. 494–502 (2013)
29. Doersch, C., Gupta, A., Efros, A.A.: Unsupervised visual representation learning by context prediction. In: ICCV. pp. 1422–1430 (2015)
30. Dosovitskiy, A., Beyer, L., Kolesnikov, A., Weissenborn, D., Zhai, X., Unterthiner, T., Dehghani, M., Minderer, M., Heigold, G., Gelly, S., Uszkoreit, J., Houlsby, N.: An image is worth 16x16 words: Transformers for image recognition at scale. In: ICLR (2021)
31. Efros, A.A.: Self-supervision for learning from the bottom up (invited talk). ICLR (2021)
32. Fei-Fei, L., Perona, P.: A bayesian hierarchical model for learning natural scene categories. In: CVPR. vol. 2, pp. 524–531 (2005)
33. Geirhos, R., Jacobsen, J.H., Michaelis, C., Zemel, R.S., Brendel, W., Bethge, M., Wichmann, F.: Shortcut learning in deep neural networks. Nature Machine Intelligence **2**, 665–673 (2020)
34. Gidaris, S., Singh, P., Komodakis, N.: Unsupervised representation learning by predicting image rotations. In: ICLR (2018)
35. Godard, C., Aodha, O.M., Brostow, G.J.: Digging into self-supervised monocular depth estimation. In: ICCV. pp. 3828–3838 (2019)
36. Goldberg, Y., Levy, O.: word2vec explained: deriving Mikolov et al.’s negative-sampling word-embedding method. ArXiv [abs/1402.3722](https://arxiv.org/abs/1402.3722) (2014)
37. Goyal, P., Caron, M., Lefaudeux, B., Xu, M., Wang, P., Pai, V., Singh, M., Liptchinsky, V., Misra, I., Joulin, A., Bojanowski, P.: Self-supervised pretraining of visual features in the wild. ArXiv [abs/2103.01988](https://arxiv.org/abs/2103.01988) (2021)
38. Goyal, P., Dollár, P., Girshick, R.B., Noordhuis, P., Wesolowski, L., Kyrola, A., Tulloch, A., Jia, Y., He, K.: Accurate, large minibatch SGD: Training ImageNet in 1 hour. ArXiv [abs/1706.02677](https://arxiv.org/abs/1706.02677) (2017)
39. Goyal, P., Duval, Q., Reizenstein, J., Leavitt, M., Xu, M., Lefaudeux, B., Singh, M., Reis, V., Caron, M., Bojanowski, P., Joulin, A., Misra, I.: VISSL. <https://github.com/facebookresearch/vissl> (2021)
40. Grill, J.B., Strub, F., Altché, F., Tallec, C., Richemond, P.H., Buchatskaya, E., Doersch, C., Pires, B.Á., Guo, Z.D., Azar, M.G., Piot, B., Kavukcuoglu, K., Munos, R., Valko, M.: Bootstrap your own latent: A new approach to self-supervised learning. In: NeurIPS. vol. 33, pp. 21271–21284 (2020)



41. Gutmann, M., Hyvärinen, A.: Noise-contrastive estimation: A new estimation principle for unnormalized statistical models. *Journal of Machine Learning Research (JMLR)* **9**, 297–304 (Jan 2010)
42. Harnad, S.: The symbol grounding problem. *Physica D: Nonlinear Phenomena* **42**(1), 335–346 (1990)
43. Harris, Z.S.: Distributional structure. *WORD* **10**(2-3), 146–162 (1954). <https://doi.org/10.1080/00437956.1954.11659520>
44. He, K., Fan, H., Wu, Y., Xie, S., Girshick, R.: Momentum contrast for unsupervised visual representation learning. In: *CVPR*. pp. 9726–9735 (2020). <https://doi.org/10.1109/CVPR42600.2020.00975>
45. He, K., Zhang, X., Ren, S., Sun, J.: Deep residual learning for image recognition. In: *CVPR*. pp. 770–778 (2016)
46. Hornik, K., Stinchcombe, M.B., White, H.L.: Multilayer feedforward networks are universal approximators. *Neural Networks* **2**(5), 359–366 (1989)
47. Hoyer, L., Dai, D., Chen, Y., Köring, A., Saha, S., Gool, L.V.: Three ways to improve semantic segmentation with self-supervised depth estimation. In: *CVPR*. pp. 11130–11140 (2021)
48. Ji, X., Henriques, J.F., Vedaldi, A.: Invariant information clustering for unsupervised image classification and segmentation. In: *ICCV*. pp. 9865–9874 (2019)
49. Johnson, J., Douze, M., Jégou, H.: Billion-scale similarity search with GPUs. *IEEE Transactions on Big Data* **7**(3), 535–547 (2019)
50. Kaiser, T., Adaloglou, N.: Understanding SwAV: Self-supervised learning with contrasting cluster assignments. <https://theaisummer.com/swav/> (2021)
51. Krizhevsky, A., Sutskever, I., Hinton, G.E.: ImageNet classification with deep convolutional neural networks. In: *NIPS*. vol. 25, pp. 1097–1105 (2012)
52. Lan, Z., Chen, M., Goodman, S., Gimpel, K., Sharma, P., Soricut, R.: ALBERT: A lite BERT for self-supervised learning of language representations. In: *ICLR* (2020)
53. LeCun, Y., Misra, I.: Self-supervised learning: The dark matter of intelligence. <https://ai.facebook.com/blog/self-supervised-learning-the-dark-matter-of-intelligence> (Mar 2021)
54. Lévy, B., Schwindt, E.L.: Notions of optimal transport theory and how to implement them on a computer. *Computers & Graphics* **72**, 135–148 (2018)
55. Liang, X., Hu, Z., Zhang, H., Lin, L., Xing, E.P.: Symbolic graph reasoning meets convolutions. In: *NeurIPS*. vol. 31, pp. 1853–1863 (2018)
56. Lin, T.Y., Dollár, P., Girshick, R., He, K., Hariharan, B., Belongie, S.: Feature pyramid networks for object detection. In: *CVPR*. pp. 936–944 (2017)
57. Lin, T.Y., Maire, M., Belongie, S.J., Hays, J., Perona, P., Ramanan, D., Dollár, P., Zitnick, C.L.: Microsoft COCO: Common objects in context. In: *ECCV*. pp. 740–755. Springer (2014)
58. Liu, Y., Ott, M., Goyal, N., Du, J., Joshi, M., Chen, D., Levy, O., Lewis, M., Zettlemoyer, L., Stoyanov, V.: RoBERTa: A robustly optimized BERT pretraining approach. *ArXiv abs/1907.11692* (2019)
59. Loshchilov, I., Hutter, F.: SGDR: Stochastic gradient descent with warm restarts. In: *ICLR* (2017)
60. Lowe, D.G.: Object recognition from local scale-invariant features. In: *ICCV*. vol. 2, pp. 1150–1157 (1999)
61. Lu, Z., Pu, H., Wang, F., Hu, Z., Wang, L.: The expressive power of neural networks: A view from the width. In: *NIPS*. pp. 6232–6240 (2017)

62. Luis, J., Bello, G., Kim, M.: Forget about the LiDAR: Self-supervised depth estimators with MED probability volumes. In: *NeurIPS*. vol. 33, pp. 12626–12637 (2020)
63. Marcus, G., Davis, E.: *Rebooting AI: Building Artificial Intelligence We Can Trust*. Pantheon Books, USA (2019)
64. Medin, D.L., Schaffer, M.M.: Context theory of classification learning. *Psychological Review* **85**, 207–238 (1978)
65. Mikolov, T., Chen, K., Corrado, G.S., Dean, J.: Efficient estimation of word representations in vector space. In: *ICLR* (2013)
66. Mikolov, T., Sutskever, I., Chen, K., Corrado, G.S., Dean, J.: Distributed representations of words and phrases and their compositionality. In: *NIPS*. pp. 3111–3119 (2013)
67. Misra, I., van der Maaten, L.: Self-supervised learning of pretext-invariant representations. In: *CVPR*. pp. 6706–6716 (2020)
68. Noroozi, M., Favaro, P.: Unsupervised learning of visual representations by solving jigsaw puzzles. In: *ECCV*. pp. 69–84. Springer (2016)
69. Nosofsky, R.M.: Attention, similarity, and the identification-categorization relationship. *Journal of Experimental Psychology* **115**, 39–57 (1986)
70. Nosofsky, R.M., Kruschke, J.K., McKinley, S.C.: Combining exemplar-based category representations and connectionist learning rules. *Journal of Experimental Psychology* **18**, 211–233 (1992)
71. van den Oord, A., Li, Y., Vinyals, O.: Representation learning with contrastive predictive coding. *ArXiv abs/1807.03748* (2018)
72. Ouali, Y., Hudelot, C., Tami, M.: Autoregressive unsupervised image segmentation. pp. 142–158 (2020)
73. Paszke, A., Gross, S., Massa, F., Lerer, A., Bradbury, J., Chanan, G., Killeen, T., Lin, Z., Gimelshein, N., Antiga, L., Desmaison, A., Köpf, A., Yang, E., DeVito, Z., Raison, M., Tejani, A., Chilamkurthy, S., Steiner, B., Fang, L., Bai, J., Chintala, S.: PyTorch: An imperative style, high-performance deep learning library. In: *NeurIPS*. vol. 32, pp. 8026–8037 (2019)
74. Pathak, D., Krähenbühl, P., Donahue, J., Darrell, T., Efros, A.A.: Context encoders: Feature learning by inpainting. In: *CVPR*. pp. 2536–2544 (2016). <https://doi.org/10.1109/CVPR.2016.278>
75. Pearson, K.: On lines and planes of closest fit to systems of points in space. *The London, Edinburgh, and Dublin Philosophical Magazine and Journal of Science* **2**(11), 559–572 (1901)
76. Pennington, J., Socher, R., Manning, C.D.: GloVe: Global vectors for word representation. In: *EMNLP*. pp. 1532–1543 (2014)
77. Peters, M.E., Neumann, M., Iyyer, M., Gardner, M., Clark, C., Lee, K., Zettlemoyer, L.: Deep contextualized word representations. In: *NAACL*. pp. 2227–2237 (Jun 2018)
78. Radford, A., Narasimhan, K., Salimans, T., Sutskever, I.: Improving language understanding by generative pre-training. In: *Open AI* (2018)
79. Ren, X., Malik, J.: Learning a classification model for segmentation. In: *ICCV*. vol. 1, pp. 10–17 (2003)
80. Rosch, E.H.: Natural categories. *Cognitive Psychology* **4**(3), 328–350 (1973). [https://doi.org/https://doi.org/10.1016/0010-0285\(73\)90017-0](https://doi.org/https://doi.org/10.1016/0010-0285(73)90017-0)
81. Singh, S., Gupta, A., Efros, A.A.: Unsupervised discovery of mid-level discriminative patches. In: *ECCV*. pp. 73–86. Springer (2012)
82. Sivic, J., Russell, B., Efros, A.A., Zisserman, A., Freeman, W.: Discovering object categories in image collections. In: *ICCV*. pp. 370–377 (2005)

83. Sivic, J., Zisserman, A.: Video Google: a text retrieval approach to object matching in videos. In: ICCV. vol. 2, pp. 1470–1477 (2003)
84. Turian, J.P., Ratinov, L.A., Bengio, Y.: Word representations: A simple and general method for semi-supervised learning. In: 48th Annual Meeting of the Association for Computational Linguistics (ACL). pp. 384–394 (2010)
85. Uijlings, J.R., Van de Sande, K.E., Gevers, T., Smeulders, A.W.: Selective search for object recognition. IJCV **104**, 154–171 (2013). <https://doi.org/10.1007/s11263-013-0620-5>
86. Vaswani, A., Shazeer, N., Parmar, N., Uszkoreit, J., Jones, L., Gomez, A.N., Kaiser, L., Polosukhin, I.: Attention is all you need. In: NIPS. vol. 30, p. 6000–6010 (2017)
87. Vu, T.H., Jain, H., Bucher, M., Cord, M., Pérez, P.: DADA: Depth-aware domain adaptation in semantic segmentation. In: ICCV. pp. 7364–7373 (2019)
88. Wang, X., Rufeng, Z., Shen, C., Kong, T., Li, L.: Dense contrastive learning for self-supervised visual pre-training. In: CVPR. pp. 3024–3033 (2021)
89. Wei, F., Gao, Y., Wu, Z., Hu, H., Lin, S.: Aligning pretraining for detection via object-level contrastive learning. In: NeurIPS. vol. 34 (2021)
90. Wen, Z., Li, Y.: Toward understanding the feature learning process of self-supervised contrastive learning. In: ICML. vol. 139, pp. 11112–11122 (2021)
91. Wu, B., Xu, C., Dai, X., Wan, A., Zhang, P., Tomizuka, M., Keutzer, K., Vajda, P.: Visual transformers: Token-based image representation and processing for computer vision. ArXiv **abs/2006.03677** (2020)
92. Xiao, T., Reed, C.J., Wang, X., Keutzer, K., Darrell, T.: Region similarity representation learning. In: ICCV. pp. 10539–10548 (2021)
93. Xiao, T., Wang, X., Efros, A.A., Darrell, T.: What should not be contrastive in contrastive learning. In: ICLR (2021)
94. Yang, C., Wu, Z., Zhou, B., Lin, S.C.F.: Instance localization for self-supervised detection pretraining. In: CVPR. pp. 3987–3996 (2021)
95. Yang, L., Cheung, N.M., Li, J., Fang, J.: Deep clustering by Gaussian mixture variational autoencoders with graph embedding. In: ICCV. pp. 6439–6448 (2019). <https://doi.org/10.1109/ICCV.2019.00654>
96. Yang, Z., Dai, Z., Yang, Y., Carbonell, J.G., Salakhutdinov, R., Le, Q.V.: XLNet: Generalized autoregressive pretraining for language understanding. In: NeurIPS. vol. 32 (2019)
97. You, Y., Gitman, I., Ginsburg, B.: Large batch training of convolutional networks. ArXiv **abs/1708.03888** (2017)
98. Zbontar, J., Jing, L., Misra, I., LeCun, Y., Deny, S.: Barlow twins: Self-supervised learning via redundancy reduction. In: ICML. pp. 12310–12320 (2021)
99. Zhan, X., Xie, J., Liu, Z., Ong, Y.S., Loy, C.C.: Online deep clustering for unsupervised representation learning. In: CVPR. pp. 6688–6697 (2020). <https://doi.org/10.1109/CVPR42600.2020.00672>
100. Zhang, R., Isola, P., Efros, A.A.: Colorful image colorization. In: ECCV. pp. 649–666. Springer (2016)
101. Zhang, S., Yan, S., He, X.: LatentGNN: Learning efficient non-local relations for visual recognition. In: ICML. pp. 7374–7383 (2019)

## A Pseudocodes

Algorithm 1 explains the generation of  $M$  views for a batch of  $N$  images. The algorithm samples an image  $X^{(n)}$  and computes a superpixel index map  $A^{(n)}$ .

$M$  views are generated from the sampled image and superpixel index map. Each of these views are randomly masked before being resized to the same pixel dimension. Only mutual regions existing in all views are kept. All views are geometrically augmented by random horizontal flipping, and appearance augmented by color distortion and randomly blurred. All generated views are gathered and converted into a 4D tensor.

---

**Algorithm 1** View generation
 

---

```

 $\tilde{X} := \{\}$  ▷ Empty sets
 $\tilde{A} := \{\}$ 
for  $n \in \{1, \dots, N\}$  do
   $X^{(n)} \sim \text{dataloader}$  ▷ Sample an image
   $A^{(n)} := \text{superpixels}(X^{(n)})$ 

   $\tilde{X}^{(n)}, \tilde{A}^{(n)} := \text{gen\_views}(X^{(n)}, A^{(n)})$ 
  #  $\tilde{X}^{(n)} = \{\tilde{X}^{(1,n)}, \dots, \tilde{X}^{(M,n)}\}$ 
  #  $\tilde{A}^{(n)} = \{\tilde{A}^{(1,n)}, \dots, \tilde{A}^{(M,n)}\}$ 

   $\tilde{X}^{(n)}, \tilde{A}^{(n)} := \text{mask\_views}(\tilde{X}^{(n)}, \tilde{A}^{(n)})$ 
   $\tilde{X}^{(n)}, \tilde{A}^{(n)} := \text{resize\_views}(\tilde{X}^{(n)}, \tilde{A}^{(n)})$ 
   $\tilde{X}^{(n)}, \tilde{A}^{(n)} := \text{mutual\_regions}(\tilde{X}^{(n)}, \tilde{A}^{(n)})$ 

   $\tilde{X}^{(n)}, \tilde{A}^{(n)} := \text{geometric\_aug}(\tilde{X}^{(n)}, \tilde{A}^{(n)})$ 
   $\tilde{X}^{(n)} := \text{appearance\_aug}(\tilde{X}^{(n)})$ 

   $\tilde{X} := \tilde{X} + \tilde{X}^{(n)}$  ▷ Add new views to set
   $\tilde{A} := \tilde{A} + \tilde{A}^{(n)}$ 
end for
 $\tilde{X} := \text{to\_tensor}(\tilde{X})$  ▷  $\tilde{X} \in \mathbb{R}^{B \times 3 \times h \times w}$ 
 $\tilde{A} := \text{to\_tensor}(\tilde{A})$  ▷  $\tilde{A} \in \mathbb{R}^{B \times 1 \times h \times w}$ 

```

---

Algorithm 2 explains the learning algorithm. The model  $f_\theta$  generates an embedding map  $\tilde{Z}$  from the image view tensor  $\tilde{X}$ . The single tensor  $\tilde{Z}$  is decomposed into  $B$  tensors  $\tilde{Z}^{(b)}$  each corresponding to a single view. Next, four trees are created to contain the latent visual embeddings  $z$  for all elements in each mutual region  $i$ . A mean vectors  $z^*$  is computed to represent regions. Each mean vector gets computed a concept compatibility score  $s^*$  as distance to each cluster  $C = (c^{(1)}, \dots, c^{(K)})$ . The swapped prediction objective is computed using the score vectors  $s^*$  stored in the tree  $T_{S^*}$ . The model parameters  $\theta$  and set of visual concept vectors  $C$  are optimized to reduce the loss  $\mathcal{L}$ .

The swapped prediction objective is explained in Algorithm 3. First, we compute an optimal assignment of visual concepts  $Q$  based on the scores in the first view  $m = 1$ . The loss is minimized when predicted visual embeddings in secondary views  $m \geq 1$  are closer to the optimally assigned visual concept vectors for each region  $i$  in all views  $m$  of all images  $n$ . This results in a cross-entropy

---

**Algorithm 2** Learning algorithm

---

```

# Generate embedding maps
 $\hat{Z} := f_\theta(\hat{X})$   $\triangleright \hat{Z} \in \mathbb{R}^{B \times D \times h \times w}$ 
 $\{\hat{Z}^{(1)}, \dots, \hat{Z}^{(B)}\} := \text{decompose}(\hat{Z})$ 

# Create embedding and score trees
 $T_Z(n, m, i) := \{\}$   $\triangleright$  Empty depth-3 trees
 $T_{Z^*}(n, m, i) := \{\}$ 
 $T_{S^*}(n, m, i) := \{\}$ 
for  $b \in \{1, \dots, B\}$  do
   $\tilde{Z}^{(b)} := \text{unroll}(\hat{Z}^{(b)})$   $\triangleright \tilde{Z}^{(b)} \in \mathbb{R}^{hw \times D}$ 
   $\tilde{A}^{(b)} := \text{unroll}(\hat{A}^{(b)})$   $\triangleright \tilde{A}^{(b)} \in \mathbb{R}^{hw}$ 
   $n, m := \text{img\_view\_index}(b)$ 
   $I := \text{num\_regions}(\tilde{A}^{(b)})$ 
  for  $i \in \{1, \dots, I\}$  do
    # Compute mean vectors for region
     $\{\hat{z}^{(j)}\} := \text{extract\_region}(\tilde{Z}^{(b)}, \tilde{A}^{(b)}, i)$ 
     $T_Z(n, m, i) := \{\hat{z}^{(j)}\}$ 
     $z^{(i)*} := \text{mean}(T_Z(n, m, i))$ 
     $T_{Z^*}(n, m, i) := z^{(i)*}$ 

    # Compute score vectors for region
     $s^{(i)*} = (T_{Z^*}(n, m, i))^T C$ 
     $T_{S^*} := s^{(i)*}$ 
  end for
end for

 $\mathcal{L} = \text{swapped\_prediction}(T_{S^*})$ 

optimize( $\theta, C, \mathcal{L}$ )

```

---

optimization objective when both assignments  $q^{(i)}$  and compatibility scores  $s^{(i)*}$  are normalized.

---

**Algorithm 3** Swapped prediction objective
 

---

```

 $\mathcal{L} := 0$ 
 $Q := \text{optimal\_assignment}(T_{S^*})$ 
for  $n \in \{1, \dots, N\}$  do
  for  $m \in \{2, \dots, M\}$  do
    for  $i \in \{1, \dots, I\}$  do
       $q^{(i)} := Q(n, i)$ 
       $s^{(i)*} := T_{S^*}(n, m, i)$ 
       $p^{(i)} := \sigma\left(\frac{1}{\tau} s^{(i)*}\right)$ 
       $\mathcal{L} -= q^{(i)} \log p^{(i)}$ 
    end for
     $\mathcal{L} := \mathcal{L}/I$ 
  end for
end for
 $\mathcal{L} := \mathcal{L}/(N(M-1))$ 

```

---

## B Hyperparameter study

We quantify the effect of hyperparameter choices by running a set of COCO representation quality experiments for four epochs. In each experiment we change only a single parameter in an otherwise static baseline configuration. The experiments are listed in Table 5. Our baseline experiment setup is as follows; view size 500 px, maximal mask coverage 50 %, 128 concepts, queue size of 5K vectors, four views, embedding dimension  $D$  equaling 64, and modest view resize range (0.5, 1.5).

The results indicate that smaller view sizes are favorable, as also noted in DINO [13]. Modest masking proves to be better than no masking. The ideal number of concepts needs to be found by experiments. Increasing the number of views improves representation learning, as also noted in SwAV [12]. Larger embedding size  $D$  results in more expressive embeddings. The benefit of increasing  $D$  is confirmed by an additional experiment using smaller 400 px view sizes to fit training jobs in GPU memory. All benchmark experiments presented in the main paper use the optimal hyperparameters found in this study.

Table 6 present COCO experiments with varying feature dimension  $D$  and number of prototypes  $K$ . Each model uses the same RN 50 backbone and is trained for 4 epochs. Increasing  $D$  consistently results in better performance. However, increasing  $K$  beyond 128 prototypes leads to worse result, at least for the same amount of training iterations. The possibility of further improving maximum performance by increasing  $D$  and  $K$  with additional training epochs remain to be explored.

**Table 5.** Hyperparameter experiments

Hyperparameter change	$\Delta$ mIoU
View size 500 $\rightarrow$ 400 px	+2.34 (+12.7%)
Masking ratio 50% $\rightarrow$ 25%	+1.52 (+8.3%)
Masking ratio 50% $\rightarrow$ 0%	+1.35 (+7.4%)
#Concepts 128 $\rightarrow$ 64	-0.45 (-2.5%)
#Concepts 128 $\rightarrow$ 256	-0.59 (-3.2%)
Queue size 5K $\rightarrow$ 10K	-0.73 (-4.0%)
#Views 4 $\rightarrow$ 3	-1.22 (-6.6%)
Emb. size $D$ 64 $\rightarrow$ 32	-1.48 (-8.1%)
Resize range (0.5, 1.5) $\rightarrow$ (0.15, 2.0)	-1.86 (-10.1%)

**Table 6.** Effect of varying feature dimension  $D$  and prototype count  $K$ 

$(D, K)$	(64, 64)	(64, 128)	(128, 128)	(128, 256)	(256, 128)	(256, 256)
mIoU	26.34	26.91	27.20	26.36	<b>27.25</b>	26.08

## C Expanded experimental results

Here we present results which are left out from the main paper due to space constraints.

**High-resolution vs. low-resolution models** Table 7 display a results of the best high- and low-resolution models evaluated on the same set of high-resolution images. For cluster evaluation models, high resolution results are consistently better than corresponding low-resolution results. For linear evaluation models, we find that training on high-resolution images increases mIoU by 1.75 on COCO [57,8]. For Cityscapes [21] we find that results decreased by 0.44. We believe that large and general image datasets like COCO benefit from the additional texture information extractable from high-resolution images. In contrast, Cityscapes is a domain-specific image dataset, for which increased resolution is known to benefit segmentation of thin and small details like poles and signs [14]. As ViCE and prior methods do not effectively distinguish such semantics in Cityscapes, it is plausible that the potential of increased resolution remains largely underutilized. Note that effectively training on high-resolution images is only possible due to superpixelization as implemented in ViCE.

**Linear model vs. cluster-based evaluation** Table 8 summarizes results of the best high- and low-resolution models evaluated on the same set of high-resolution images. The linear evaluation models performs better across the range

**Table 7.** Performance of best models trained on high- and low-resolution images

Dataset	Resolution	Configuration	Cluster mIoU	Linear mIoU
COCO	Low	RN50, FPN	19.37	27.63
	High	RN50, DLV3+	21.77	29.38
Cityscapes	Low	RN18, FPN	21.48	30.84
	High	RN18, DLV3+	25.23	30.40

of cluster and filter counts, in contrast to our baseline PiCIE [19] which indicate comparable performance for cluster and linear model evaluation. We view this as further evidence for the enhanced task-specific interpretability and semantic consistency of our embeddings. We note that training on high-resolution images provide a consistent performance benefit for both clustering and linear evaluation models. In Table 8 the column “#” denotes the number of clusters and linear filters in the evaluation model.

**Table 8.** Performance with varying number of evaluation clusters and linear filters

Dataset	Resolution	Configuration	#	Cluster mIoU	Linear mIoU
COCO	Low	RN50, FPN	27	10.86	25.93
			45	14.04	26.43
			128	18.30	27.22
			256	19.37	27.63
	High	RN50, DLV3+	27	12.77	27.78
			45	14.98	27.77
			128	20.30	28.47
			256	21.77	29.38
Cityscapes	Low	RN18, FPN	27	19.52	26.79
			45	20.39	27.94
			128	21.48	30.27
			256	21.24	30.84
	High	RN18, DLV3+	27	20.61	28.95
			45	22.04	29.44
			128	24.24	30.02
			256	25.23	30.40

**Representation learning from random initialization** In Fig. 7 we show that ViCE is capable to learn visual concepts from scratch using both high- and



low-resolution images. In particular, the low-resolution Cityscapes model shows linear improvement and achieves 26.05 mIoU after 144 epochs, approaching the best result 30.84 mIoU obtained after 24 epochs starting with pretrained weights. Our method is thus not fundamentally reliant on weight initialization from other supervised or self-supervised pretraining tasks, though using pretrained weights effectively bootstraps learning.

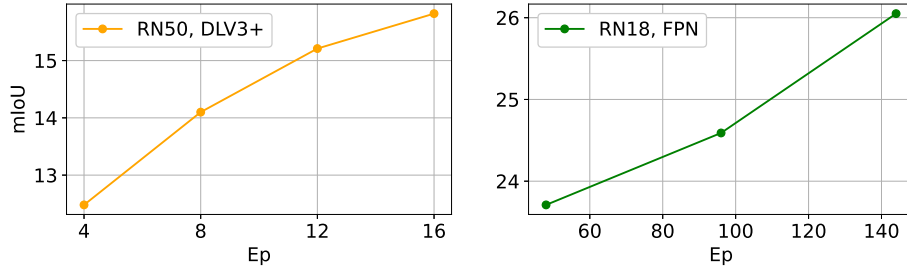


**Fig. 7.** Performance when starting from random initialization on high-resolution COCO (left) and low-resolution Cityscapes (right) images

**Effect of backbone complexity** In Fig. 8 we show how performance change with increasing backbone complexity. Our results on COCO indicate that performance per epoch consistently improves with increased backbone complexity. In contrast, the results on Cityscapes indicate worse performance. A plausible explanation is that Cityscapes is smaller and less general than COCO, making larger self-supervised models prone to overfit patterns which do not generalize beyond the training sample distribution.

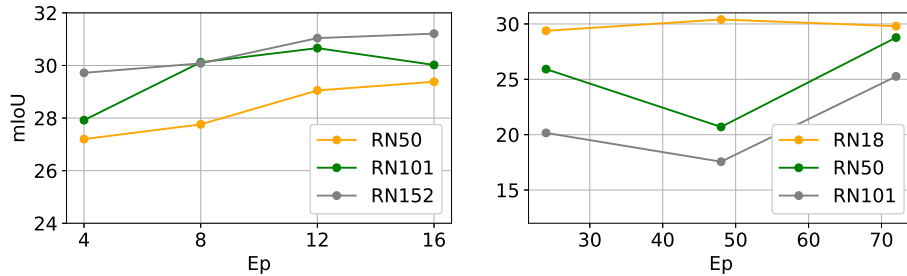


**Fig. 8.** Performance with different backbones on high-resolution COCO (left) and Cityscapes (right) images

**Domain generalization** In Table 9 we demonstrate how ViCE benefit from learning from a large visual data domain. We find that training on COCO and evaluating on Cityscapes increases mIoU by 3.74 points. Analyzing the class-wise IoU values under “DG linear” in Table 10 indicate that learning from diverse visual data enriches semantic information for minor classes like “Pole”, “Traffic sign”, “Person”, and “Bicycle”. We believe this result is a promising indicator for usefulness as a general visual models that enable learning domain-specific tasks with little supervision.

**Table 9.** Domain generalization performance

Training data	Evaluation data	mIoU	aAcc
Cityscapes	Cityscapes	30.40	87.00
COCO	Cityscapes	<b>34.14</b>	86.10

**Analysis of discovered semantics** Table 10 presents Cityscapes evaluation model results showing what semantics are readily inferrable from the learned visual concept embeddings. We find that the linear evaluation model performs better on dominant classes like “Building”, and also vague classes like “Wall”, than the clustering model. Neither evaluation model is able to distinguish between the visually similar “Person” and “Rider”. We believe this exemplifies the inherent limitation of interpreting visual concept embeddings without considering the notion of action and surrounding context.

**Downstream task evaluation** Our primary motivation for pursuing unsupervised semantic segmentation is the ability to partitioning images into a small set of semantic visual concept embeddings. Nevertheless, we also investigate the usefulness of the learned model in terms of a conventional computer vision tasks. In Table 11 we present results for supervised semantic segmentation on the COCO-Stuff164k dataset [57,8] with 27 classes [48]. We conduct experiments with randomly sampled image subsets to estimate few-shot learning performance for a DeepLabV3+[15] model with a ResNet 50 [45] backbone. The first set of experiments are initialized with the default PyTorch [73] weights, obtained through conventional supervised learning on ImageNet [26]. The second set of experiments are initialized with weights from a ViCE model.

Our hypothesis is that the feature embedding dimension difference is why unsupervised ViCE pretraining is outperformed by supervised ImageNet pretraining [26] beyond few-shot learning. Conventional unsupervised pretraining is based on classification on a single 2048 dimensional image embedding, while ViCE generates a dense 128 dimensional embedding maps. Our result indicate

**Table 10.** Class-wise performance on Cityscapes

Class	Cluster IoU	Linear IoU	DG linear IoU	Cluster Acc	Linear Acc
Road	89.12	91.81	87.23	95.02	96.20
Sidewalk	39.65	49.58	34.38	60.26	65.62
Building	75.59	78.25	77.87	90.40	92.86
Wall	0.0	7.79	7.60	0.0	8.47
Fence	0.0	5.67	5.48	0.0	6.68
Pole	10.65	12.23	21.81	14.64	13.68
Traffic light	0.0	0.30	1.86	0.0	0.31
Traffic sign	0.0	2.64	20.0	0.0	2.76
Vegetation	79.94	83.82	84.65	91.37	92.95
Terrain	6.87	21.73	21.79	7.69	32.65
Sky	78.66	86.77	85.10	83.48	92.35
Person	30.28	37.96	62.15	46.01	67.56
Rider	0.0	0.0	6.82	0.0	0.0
Car	68.63	77.60	76.50	90.93	92.48
Truck	0.0	0.60	0.24	0.0	0.61
Bus	0.0	2.19	0.40	0.0	2.27
Train	0.0	0.07	0.25	0.0	0.07
Motorcycle	0.0	0.0	1.22	0.0	0.0
Bicycle	0.0	18.60	53.24	0.0	22.25
mIoU, aAcc	25.23	30.40	34.14	84.28	87.00

that it is possible to learn how to utilize the rich semantics for the segmentation task with about 1000 training samples. We conclude that increasing the output feature dimension, while maintaining computational efficiency, is a promising direction to improve ViCE. Note that ViCE and other unsupervised semantic segmentation methods are capable of partitioning images into distinct concepts and clusters, which is not possible to do with a pretrained ImageNet model alone.

Unfortunately we could not include PiCIE [19] in this experiment, as the ResNet model implementation does not correspond to the standard Pytorch implementation, complicating integration into MMSegmentation [20]. However, PiCIE presents a similar experiment where they retrain models on all COCO training samples using conventional supervised learning with clustering instead of conventional linear feature interpretation. Initializing from PiCIE results in 32.81 mIoU while the ImageNet model achieves 31.51 mIoU. These values are about half of the results achieved in our experiments. We find the choice to evaluate performance using clustering to be curious decision, as the results arguably do not demonstrate real-world usefulness as a means to achieve maximum performance, which we demonstrate in the few-shot learning regime.

**Table 11.** Semantic segmentation performance with different initializations and ratio of used training samples

Ratio	0.1 %	1 %	5 %	25 %	50 %	100 %
Samples	49	496	2,481	12,407	28,814	49,629
Supervised	25.50	40.11	<b>48.05</b>	<b>54.42</b>	<b>55.68</b>	<b>58.11</b>
ViCE	<b>26.44</b>	<b>40.17</b>	47.70	54.22	55.44	57.99

**Timing information** We present training step timing information in Table 12. The summary is compiled by the framework VISSL [39], and represent average values for a training process involving 32 V100 GPUs distributed over 8 nodes. Table 13 shows average inference time per image for cluster and linear evaluation models using a single 3080Ti GPU in a desktop machine. Note that for high-resolution images, linear model evaluation is 160 times quicker than cluster evaluation implemented using FAISS [49].

**Table 12.** Average training step time per high-resolution image batch

Phase	Forward	Loss comp.	Backward	Optimization	Tot.
[msec]	429	166	4167	43	4824

**Table 13.** Average inference time for a high-resolution image

	Segmentation model	Cluster model	Linear model
[msec]	57	2395	15

## D Additional visualization results

In Fig. 9, the center image shows how visual concept embeddings in the output embedding map can be clustered into coherent regions. The right image demonstrates how to semantically interpret the image by assigning each cluster a semantic meaning or class. The fact that this is possible depends on the consistent semantic interpretability of the discovered clusters over different samples.

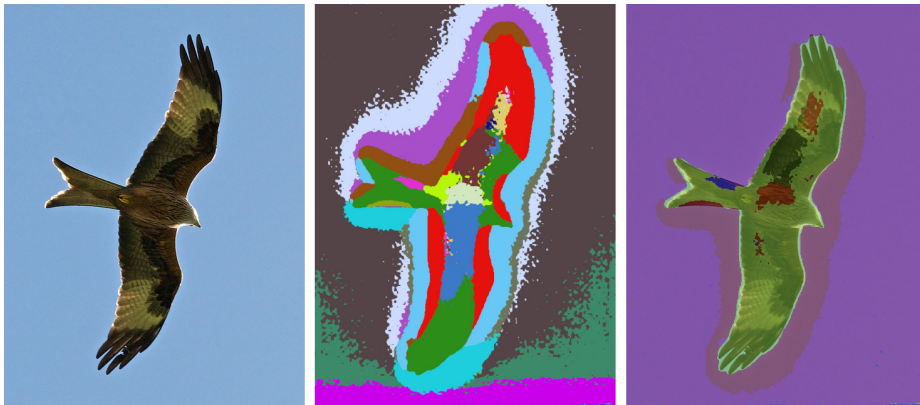


**Fig. 9.** Visualization of output clustering. The center image shows clusters with random colors. The right image shows how clusters are mapped to a single semantic class

Fig. 10 presents additional output visualizations of high-resolution COCO images for clustering and linear evaluation models with 256 clusters or linear filters. Each image is interpreted by five different models and arranged in groups. Each group display the input image in the top-left corner with the PiCIE output visualization bellow for comparison. The remaining visualizations display the output of clustering and linear evaluation models trained on high- and low-resolution COCO images. Ground truth labels are visualized in the right column. We find that high-resolution models produce better segmentation borders and less noise. Linear evaluation model output also display better segmentation borders and less noise, in addition to 160 times faster evaluation time.

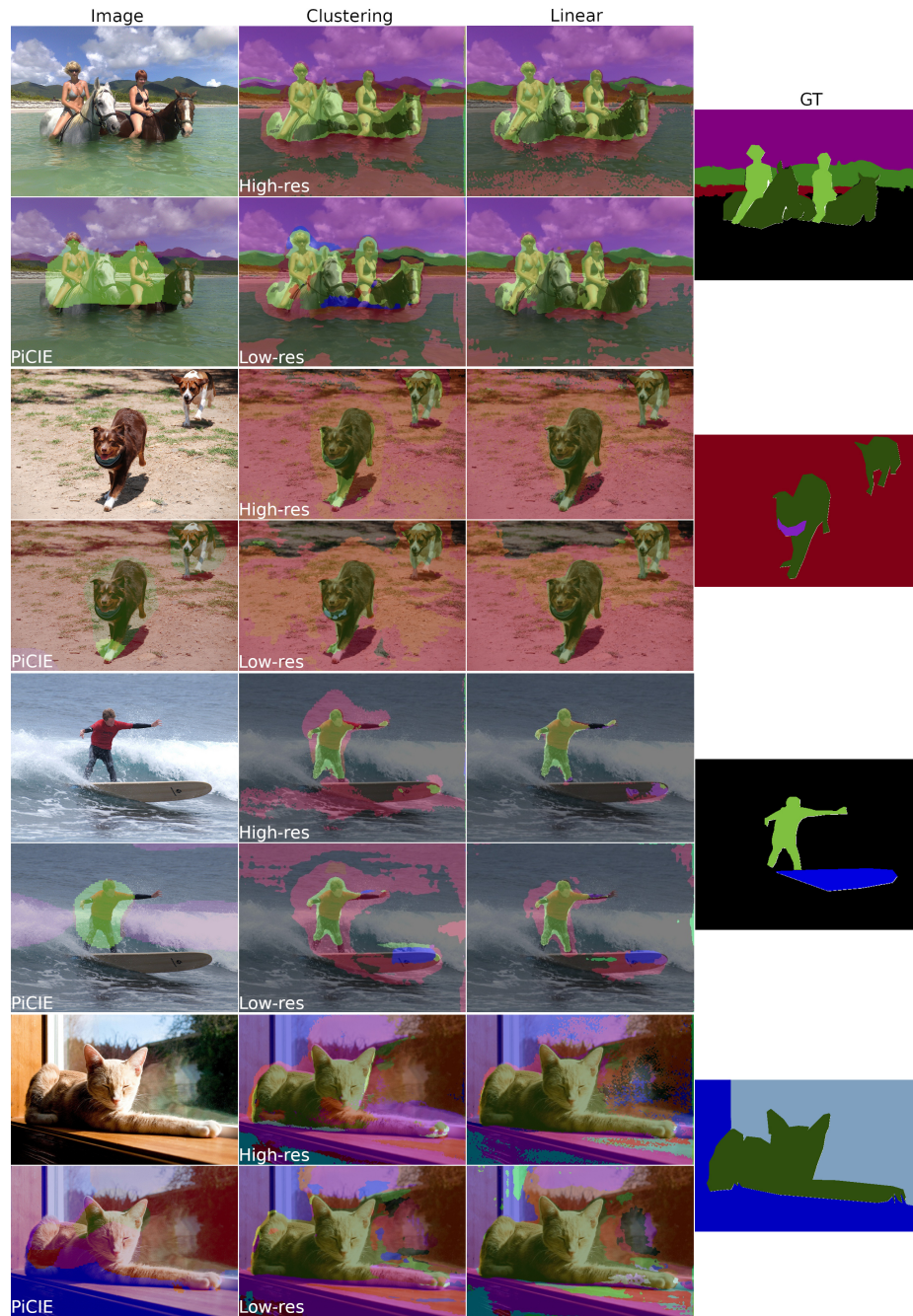


**Fig. 10.** Output visualizations of cluster and linear evaluation models trained on low- and high-resolution COCO images